applied sciences

MDPI

Article

Vertical Electrical Sounding (VES) Technique to Map Potential Aquifers of the Guigou Plain (Middle Atlas, Morocco): Hydrogeological Implications

Said El Makrini [1,*], Mustapha Boualoul [1], Younes Mamouch [2,*], Hassane El Makrini [1], Abdelhamid Allaoui [1], Giovanni Randazzo [3], Allal Roubil [4], Mohammed El Hafyani [4,5], Stefania Lanza [6] and Anselme Muzirafuti [3,*]

1 CartoTec Team, Faculty of Sciences, Moulay Ismaïl University, BP 11201 Zitoune, Meknes 50000, Morocco
2 Laboratory Physico-Chemistry of Processes and Materials, Research Team Geology of the Mining and Energetics Resources, Faculty of Sciences and Technology, Hassan First University of Settat, Settat 26002, Morocco
3 Dipartimento Scienze Matematiche e Informatiche, Scienze Fisiche e Scienze della Terra, Università Degli Studi di Messina, Via F. Stagno d'Alcontres, 31-98166 Messina, Italy
4 Laboratory of Geoengineering and Environment, Research Group "Water Sciences and Environment Engineering", Department of Geology, Faculty of Sciences, Moulay Ismail University, BP11201, Meknes 50050, Morocco
5 ULiège (Gembloux Agro-Bio Tech), Terra Research Center, Water-Soil-Plant Exchange, 5030 Gembloux, Belgium
6 GeoloGIS s.r.l., Dipartimento di Scienze Matematiche e Informatiche, Scienze Fisiche e Scienze Della Terra, Università Degli Studi di Messina, Via F. Stagno d'Alcontres, 31-98166 Messina, Italy
* Correspondence: said.elmakrini@edu.umi.ac.ma (S.E.M.); y.mamouch@uhp.ac.ma (Y.M.); anselme.muzirafuti@unime.it (A.M.)

Abstract: Vertical electrical sounding (VES) as a geoelectrical method has proven its effectiveness throughout the history of groundwater geophysical investigation. In this sense, VES was carried out 47 in the study area with the aim of determining the geometry and limits of Quaternary basaltic aquifer formations and, above all, the location of electrical discontinuities in the area located in the north of Morocco, between the center of Almis Guigou and the city of Timahdite. This area is experiencing an overexploitation of the groundwater due to excessive pumping and the development of intensive agriculture activities, resulting in a continuous decrease in piezometric levels. The processing of the diagrams by WINSEV software showed the presence of an electrically resistant surface level, attributed to basaltic formations, of the Quaternary age, whose thicknesses reach at least 150 m to the SW of the area. This level is superimposed on a moderately conductive horizon which, according to local geology, corresponds to Pliocene marl and limestone alternations. The correlation of VES interpretation models allowed us to elaborate thematic maps and geoelectrical sections which illustrate the vertical and lateral extension of the basaltic reservoir as well as its thickness, which decreases in general from the south-west to the north-east; however, the main electrical discontinuities also correspond to faults and fractures, and they show a NE–SW direction sub-parallel to the major accidents of the Middle Atlas. A prospectivity map of the local aquifer was generated, coinciding with regional fault lines and confirmed by the alignment of very good flowing water boreholes. This geophysical study by electrical sounding shed light on the geometry and extension of the aquifer and opened avenues to draw further conclusions on its physical and hydrodynamic characteristics, as well as to optimize the future siting of groundwater exploitation boreholes through the elaboration of the local aquifer prospectivity map.

Keywords: vertical electrical sounding; groundwater; hydrogeophysics; Tabular Middle Atlas; applied geophysics; agriculture; Morocco

Citation: El Makrini, S.; Boualoul, M.; Mamouch, Y.; El Makrini, H.; Allaoui, A.; Randazzo, G.; Roubil, A.; El Hafyani, M.; Lanza, S.; Muzirafuti, A. Vertical Electrical Sounding (VES) Technique to Map Potential Aquifers of the Guigou Plain (Middle Atlas, Morocco): Hydrogeological Implications. *Appl. Sci.* **2022**, *12*, 12829. https://doi.org/10.3390/app122412829

Academic Editor: Filippos Vallianatos

Received: 11 November 2022
Accepted: 12 December 2022
Published: 14 December 2022

1. Introduction

The plain of Guigou, located in the center of Morocco between the town of Timahdite and the village of Almis Guigou, has seen an important development in agricultural activities in recent decades, especially in the production of potatoes and onions, which are very well known and in demand in the Moroccan market. Indeed, this crop, which is very demanding in terms of irrigation water, is at the origin of the overexploitation of the water table in the said region. This need is manifested by the decrease in pumped flows and, consequently, the phenomenal drop in the piezometric level [1].

In this respect, detailed knowledge of the aquifer system is of great interest for the optimal management of groundwater resources in such a region [2–6]. The aquifer exploited in the region is formed by Plio-Quaternary basalts with Miocene and Cretaceous marl and limestone formations as a semi-impermeable bedrock. The fracturing affecting these basalts plays a key role in the circulation of groundwater and impacts the productivity of hydrogeological boreholes. In addition, there are few hydrogeological studies of the Plio-Quaternary basaltic aquifer in the region [1,7], and there are none based on geophysical surveys, which means that this aquifer is still poorly known and needs to be explored in detail.

The geoelectrical method, with its three most widely used techniques (tomography, profiling and vertical drilling), has long been considered the most widely used geophysical method for the characterization of aquifer systems in the world [8–21].

Due to its simplicity of implementation and cost-effectiveness compared to other methods, the vertical electrical sounding (VES) technique has proven to be very useful in mapping aquifer systems, the geological layers forming their impermeable bedrock and the detection of structural anomalies corresponding to faults and fractures [4,22–25].

In this study, we used the vertical electrical sounding (VES) technique to map the aquifer system of the Guigou plain. The main objectives of this study included the following: (i) to identify the electrical horizons of the subsoil; (ii) to determine the geological layers forming the aquifer; (iii) to determine the geometry of the aquifer system; (iv) to estimate the depth of the impermeable bedrock; and (v) to locate the geoelectrical discontinuities and determine their role in groundwater drainage.

2. Geological Background

The Moroccan Middle Atlas, shown in Figure 1, where our study area is located, is a chain structured during the Alpine orogeny. It is subdivided into two units: to the west is the Tabular Middle Atlas (TMA) unit, and to the east is the Folded Middle Atlas (FMA) unit [26,27]. The passage between these two units is underlined by a network of faults called the North Middle Atlas accident (NMAA). The Guigou plain is located at the south-eastern edge of the TMA and along the NE–SW NMAA [27–29]. It corresponds to a collapse ditch about 5 km wide and 40 km long, essentially filled with volcanic lava and traversed by Oued Guigou, which constitutes its alluvial plain [1,7,30]. The chronological succession of the geological formations of the Middle Atlas begins with the sandstone-pelitic series constituting a base attributed to the Paleozoic era, which is structured by the Hercynian orogeny [26,31–35]. In angular discordance, a thick series from the Triassic age composed of lower and upper argillites and framing a basaltic complex of doleritic-type rocks rests on this base [28,35–37]. This series is underlain by the carbonate formations of the Lias, which are interspersed with marl and limestone of the Dogger age to the Mio–Pliocene age [32]. Locally at TMA, the Quaternary period is represented by volcanic lavas of a basaltic nature. These lavas come from craters located to the north of the study area, the most important of which are Jbel Habri, Chedifat and Bou-Ahsine [28,38]. At their exit, following the example of our study area in the Guigou plain, these lava flows used the slopes to occupy the depressions [28,38]. In this plain, in addition to these basalt flows which predominantly outcrop, there are also some marl and limestone formations from the Mio-Pliocene period which outcrop mainly in the NE part in the form of small plateaus at the foot of the folded Middle Atlas [7,34].

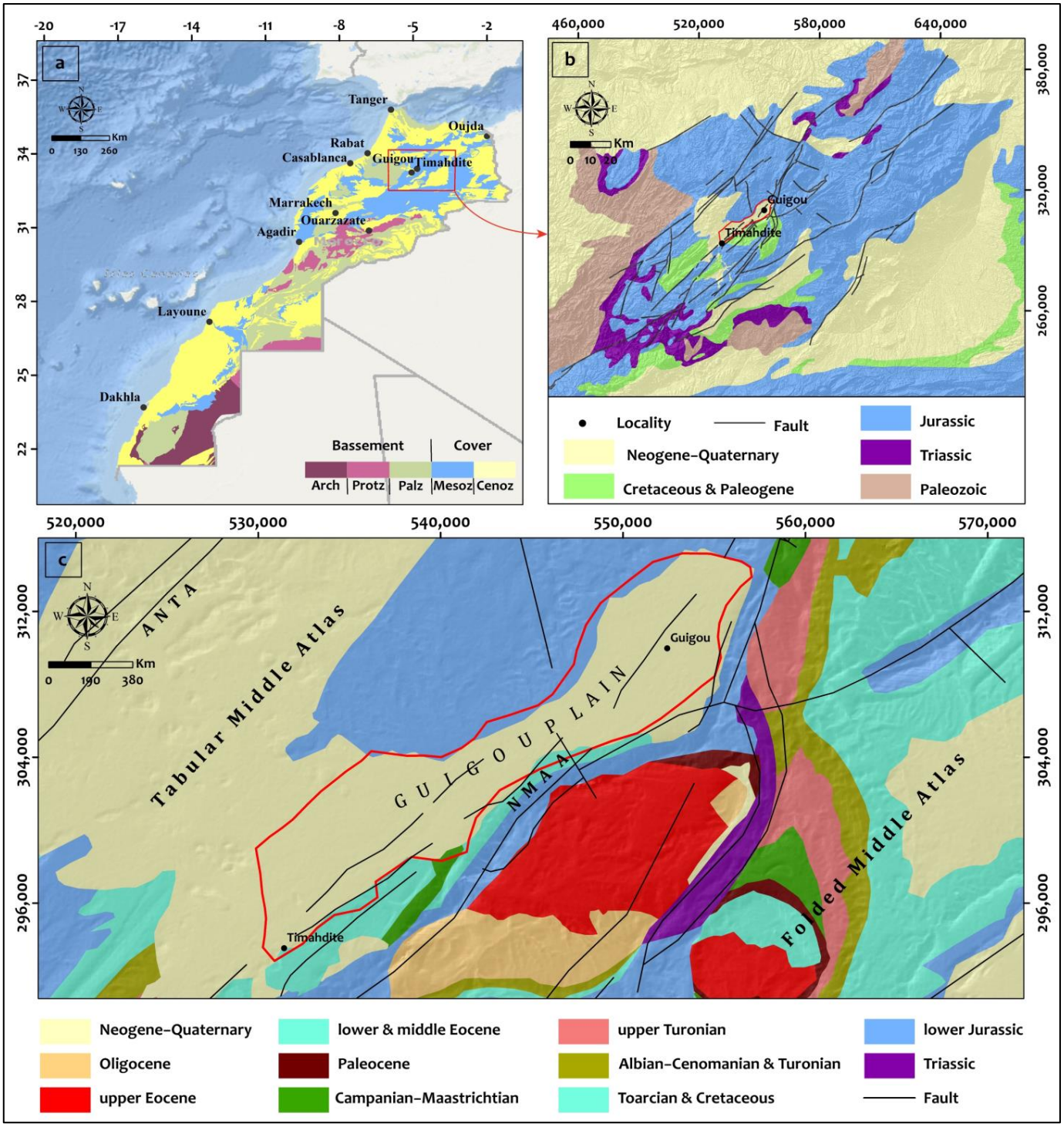

Figure 1. (**a**) General geological map of Morocco showing the location of the Middle Atlas Mountain; (**b**) Simplified geological map of the Middle Atlas extracted from the geological map of Morocco at 1/200,000, showing the location of the study area; (**c**) Sketch of the geological map of the Middle Atlas where the study area marked by the red polygon.

Tectonically, the TMA is characterized by brittle rather than folded deformation [7,28,33,39]. Indeed, two major fault networks can be distinguished, namely the NMAA fault network and the Tizi-n-Tretten (TNTA) fault network with a NE–SW direction. These two major accidents are part of the same fault system inherited from the Hercynian orogeny, which was replayed several times during the Alpine orogeny [26,40,41]. These faulted structures

that shape the TMA are easily mapped on the ground, except in areas covered by basaltic flows [28,38].

3. Materials and Methods

3.1. Vertical Electrical Sounding (VES) Basic Principle and Data Acquisition

The geoelectrical method, using the vertical electrical sounding (VES) technique, consists of measuring the variations in apparent resistivity (ρa) as a function of depth. In principle, the measurement protocol consists of injecting an electric current of intensity (I) through two current electrodes (A and B) and measuring the potential differences (ΔV) created between the two receiving electrodes (M and N), called potential electrodes (Figure 2).

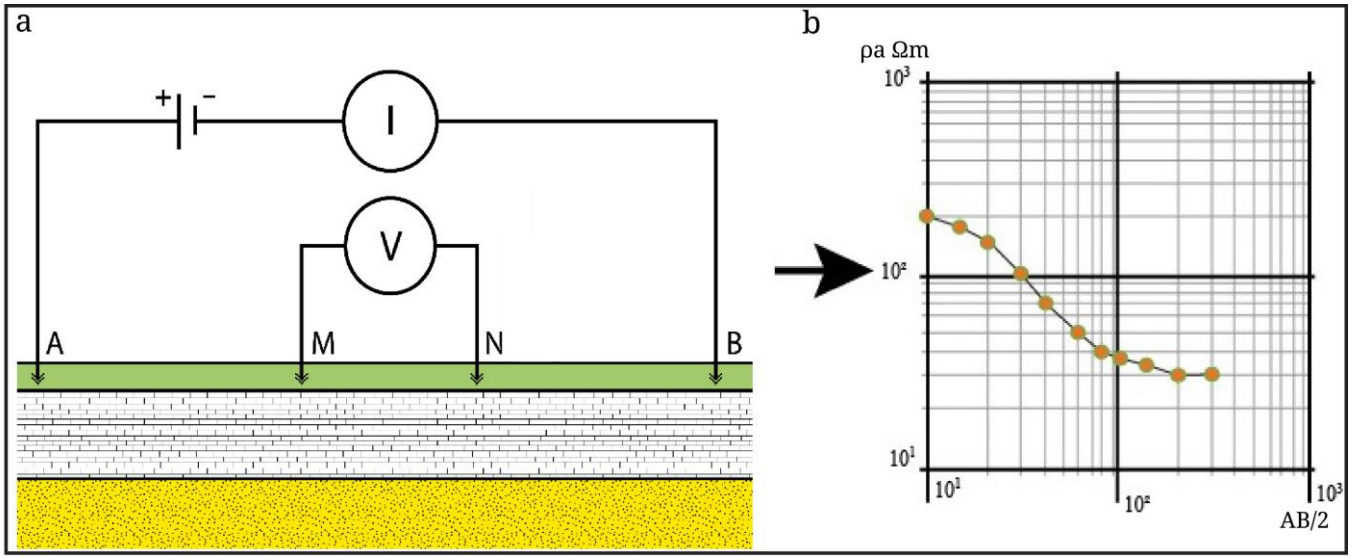

Figure 2. (**a**) General scheme of a soil-resistivity measurement using the Schlumberger configuration with a four−electrode device (ABMN), (**b**) bi−logarithmic diagram for the representation of VES measurements.

According to Ohm's law, the apparent resistivity is a function of ΔV, I and the geometric coefficient (K). It is calculated by the following formula:

$$\rho_a = \frac{\Delta V}{I} * K \text{ And } K = 2\pi \left(\frac{1}{\frac{1}{AM} + \frac{1}{AN} + \frac{1}{BM} - \frac{1}{BN}} \right)$$

The curve $\rho_a = f\left(\frac{AB}{2}\right)$ is obtained by plotting the apparent resistivity values ρ_a against AB/2 (half spacing of the current electrodes, which can reach up to 10^1 km) in a bi-logarithmic scale.

In the present study, the measurement of VES data at forty-seven stations was carried out and arranged according to seven profiles that were generally oriented NW–SE, perpendicular to the general direction of the flow of the volcanic lava. The coordinates of the measurement stations were taken by a Garmin MAP-64 s GPS. A Syscal Pro resistivity meter was used to acquire geoelectrical data. This automated instrument is powerful in DC electrical readings with the transmitter and receiver integrated in the same instrument. The measurements were made using the Schlumberger configuration. The distance between the current injection electrodes (AB) varied logarithmically from 6 to 1000 m for each measuring station. The position of the measuring stations was organized according to the profiles with a spacing of 3 to 5 km between them (Figure 3). The direction of the spread of the power cables was NE–SW, in the same direction as the regional fault system, to avoid polarity reversals created by the presence of faults or anomalous geological contacts. At the same

time, measurements of the piezometric level of the water table using a 200 m piezometric probe were acquired.

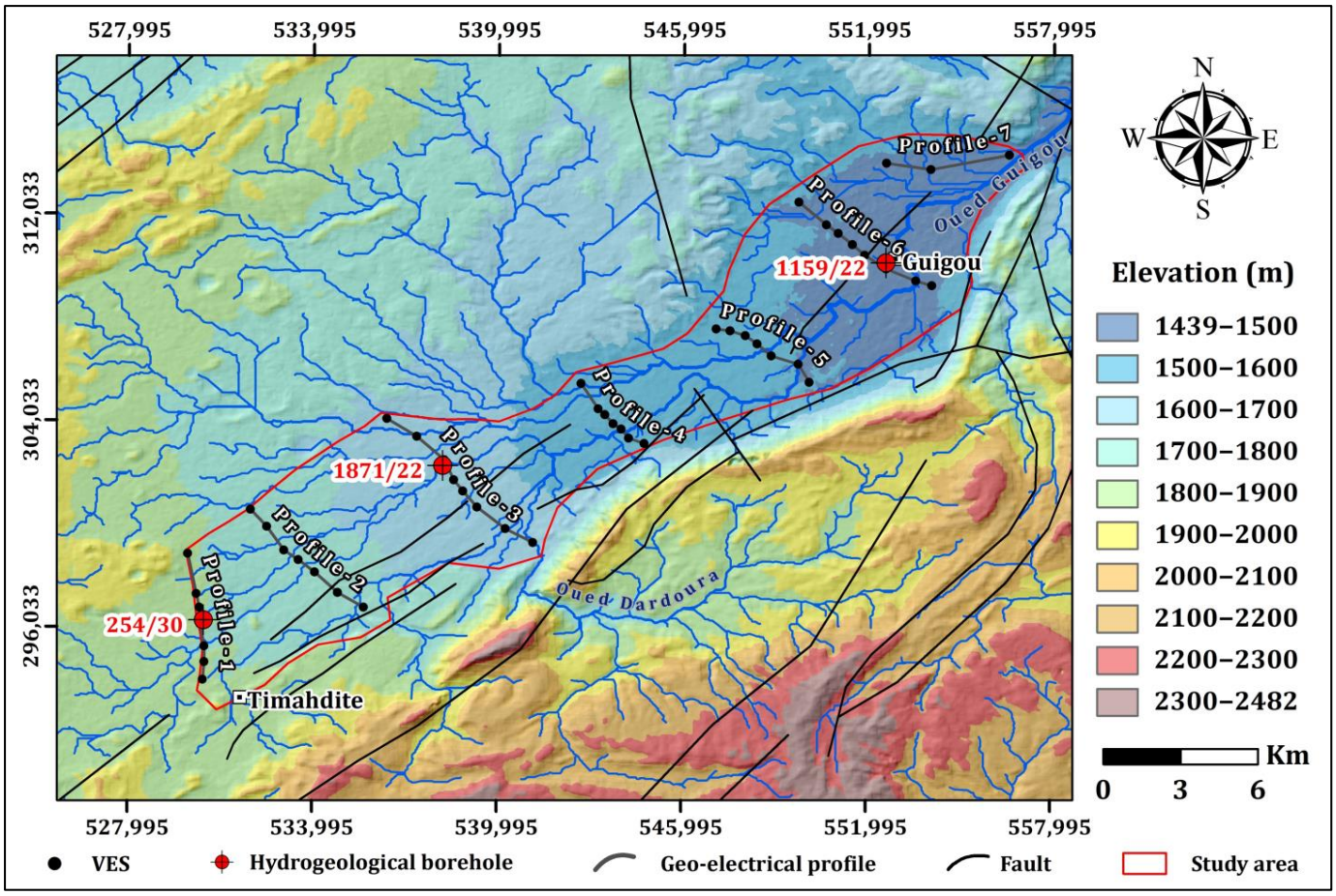

Figure 3. Position plan of VES profiles on digital terrain model.

3.2. Data Processing and Resistivity Interpretation

The VES data acquired were subjected to a series of processing steps to facilitate their interpretation, summarized in four steps. In the first step, the VES diagrams were first smoothed to eliminate all outliers. They were then inverted using Geosoft's Winsev software, which allows each diagram to be broken down into well-defined electrical levels in terms of thickness and resistivity. The models of the VES diagrams were calibrated by lithological logs of the three existing hydrogeological boreholes (Figure 3). In the second step, the geoelectric levels of the VES models of each profile (Figure 3) were correlated horizontally. Consequently, four geoelectrical sections were drawn up to follow the evolution of the resistivity and the thickness of the formations crossed in both the vertical and lateral directions. Then, the third step was to interpolate the VES data using the inverse distance weighting (IDW) method. Four thematic maps were produced, including two iso-resistivity maps, a bedrock-depth map and a thickness map of the main reservoir. Finally, based on the main geoelectrical characteristics extracted from the geoelectrical sections and maps, coupled with the available geological information, the fourth step concerned the elaboration of the groundwater prospectivity map. Figure 4 shows the methodological flowchart applied in this work, described in the four steps above.

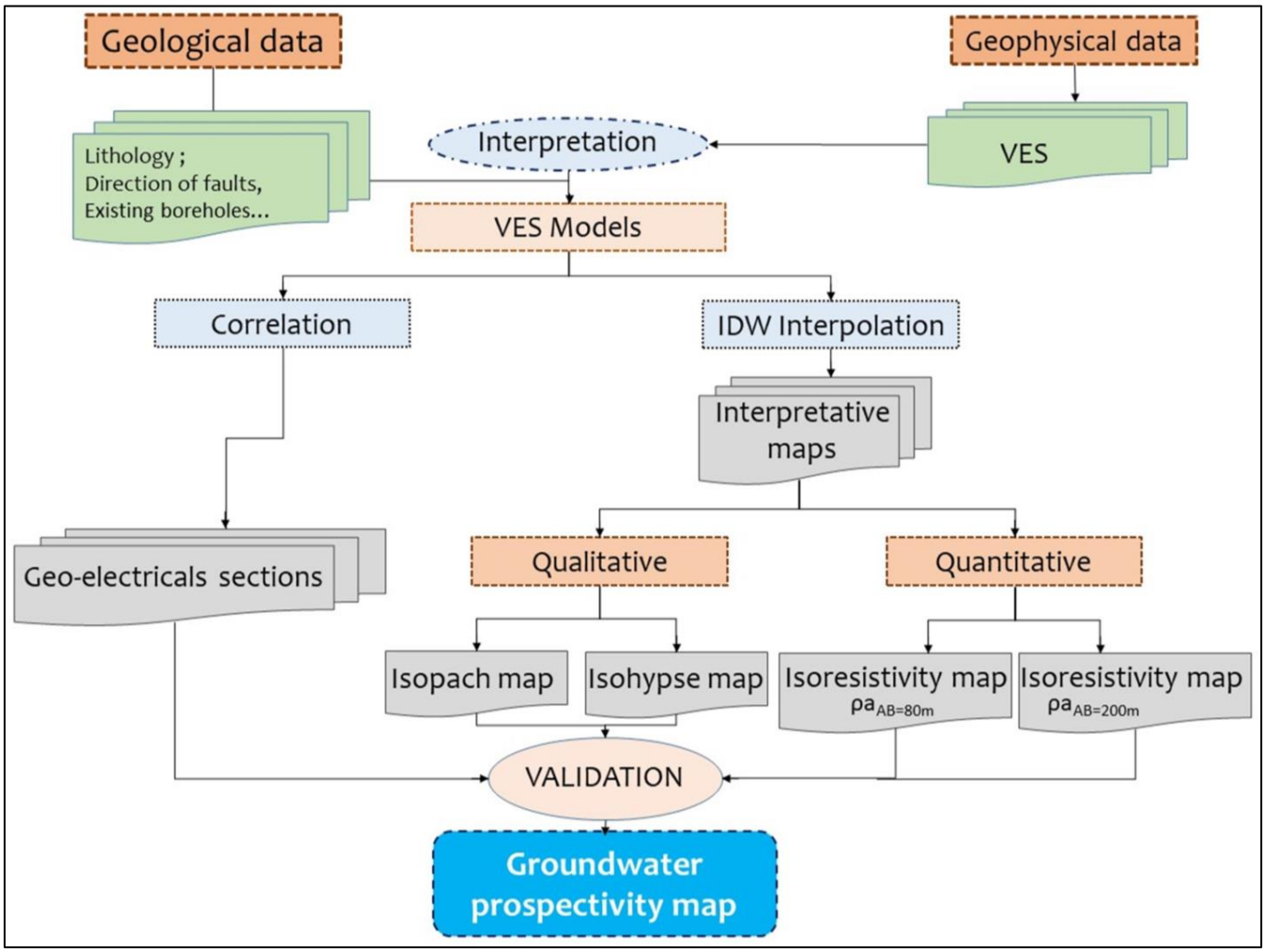

Figure 4. The methodological flowchart used in this study.

4. Results and Discussion

4.1. Geological Significance of Resistivities and VES Categories

The processing and analysis of the electrical boreholes made it possible to identify three categories of VES (C1, C2 and C3), characterizing the whole study area, based on the shape of the curve and the succession of electrical levels (resistant, conductive, two-layer intermediates, etc.). The table below gives a summary of the inversion results and the interpretation of typical VES in each category (Figure 5).

The first category, C1, was the most dominant, containing a total of 30 VES measurements. A typical VES curve is represented by the 4P1 diagram (Figure 5). The interpretation of the latter is based on the lithological data from borehole 254/30. The diagram of VES4P1 shows, from bottom to top, the presence of the following geoelectric levels (Figure 5): (i) a relatively conductive bedrock with a resistivity of 170 Ωm, located at a depth of 152 m and attributed to fairly compact Pliocene marlstone; (ii) a moderately resistant level of 450 Ωm resistivity and a thickness of 75 m that can be made to correspond to water-bearing basalts; (iii) a very resistant complex formed by two levels, a first lower level of with a resistivity of 2043 Ωm and a thickness if 55 m, which could correspond to dry and fairly compact basalts, surmounted by an upper level with a resistivity of 1347 Ωm and a thickness of 21 m, most probably attributed to weathered basalts on the surface; and (iv) a superficial level that is 2 m thick, representing the vegetal soil.

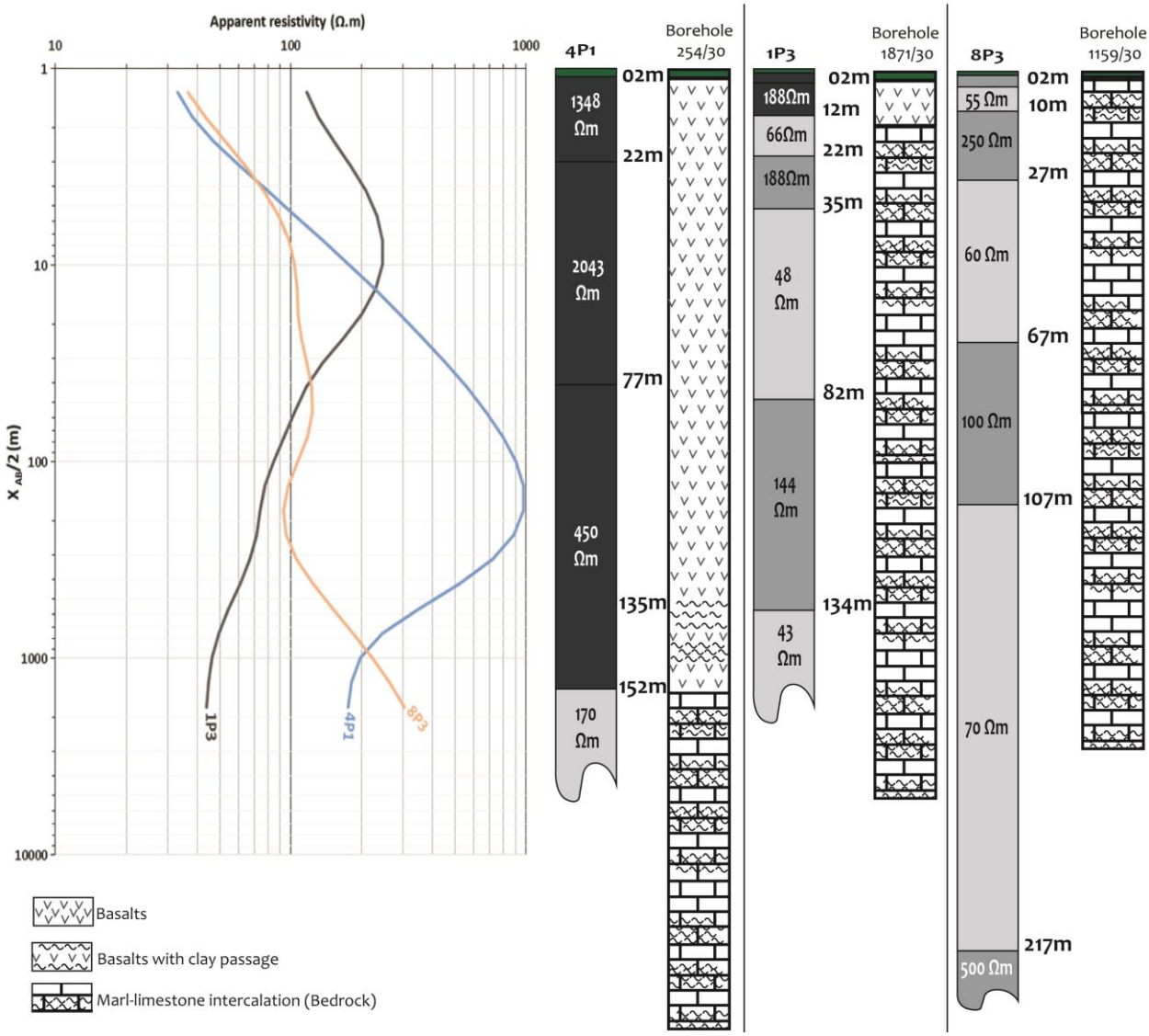

	C1 (4P1)			C2 (1P3)			C3 (8P3)		
	RESISTIVITY (Ωm)	THICKNESS (m)	DEPTH (m)	RESISTIVITY (Ωm)	THICKNESS (m)	DEPTH (m)	RESISTIVITY (Ωm)	THICKNESS (m)	DEPTH (m)
ϱ1	28	1.4		100	1.2		30	1	
ϱ2	1347	21	1.4	500	2.5	1.2	200	3	1
ϱ3	2043	55	22	150	8	3.7	55	6	4
ϱ4	450	75	64	52	10	12	250	17	10
ϱ5	170		152	177	13	22	60	40	27
ϱ6	_	_	_	42	47	35	100	40	67
ϱ7	_	_	_	144	52	82	70	100	107
ϱ8	_	_	_	46		134	500		207

Figure 5. Diagrams and interpretation models of typical SEV of each category and the borehole data with its corresponding lithological logs.

The second category (C2) contained a total of 9 VES measurements. This category is represented by the diagram of 1P3, the typical shape of the curves of which is given in Figure 5. An examination of the 1P3 diagram shows, from bottom to top, the presence of

the following geoelectrical levels: (i) a succession of moderately conductive to resistant levels, with resistivity varying between 40 Ωm and 177 Ωm, and thickness being 122 m, which corresponds to the marl–limestone intercalation of the Pliocene; and (ii) a 12 m thick resistant ensemble representing the Quaternary basalts, which were altered at the beginning, then dry before becoming slightly damp afterwards.

The third category (C3) contained a total of 08 VES measurements. The curve of the electrical borehole 8P3 (Figure 5), which is the representative of this category, shows, from bottom to top, the presence of the following geoelectrical levels: (i) a very resistant substratum with a resistivity of 500 Ωm. It is also very deep, located at a depth of 207 m, and could be the equivalent of Pliocene limestone and sandstone or any underlying formation (e.g., Jurassic limestones); (ii) a succession of moderately conductive to resistant levels, from resistivities of 50 Ωm to 250 Ωm, and 206 m thick, which would correspond to Pliocene marl and limestone; and (ii) a superficial conductive level, 1 m thick, which can be made to correspond to the vegetal soil.

4.2. Geoelectrical Section Analysis

Geoelectrical sections (GSs) yield the visualization of lateral and vertical variations of resistive and conductive horizons, as well as possible electrical discontinuities. Based on the correlation between the interpreted and inverted VES patterns, seven GSs were performed along the N–S, NW–SE and E–W directions.

It should be noted that due to the sometimes-large distance between electrical soundings in the same profile, correlations may be influenced by the presence of structural discontinuities, such as faults and fractures, making it difficult to correlate, which requires calibration with existing borehole data.

Only the four most representative cuts of these directions are presented and discussed in this work, namely GS1 (Profile 1), GS2 (Profile 3), GS3 (Profile 5) and GS4 (Profile 7). Figures 6–9 show these geoelectrical cross-sections and for each one, a simplified cross-section has been drawn with the same horizontal and vertical scale.

Section GS1, grouping the VES of profile 1 (Figure 6), shows the gradual plunge of the marl–limestone bedrock towards the north and, consequently, an increase in the thickness of the basaltic flow from the south to the north. The presence of the North Middle Atlas accident (NMAA) and the corresponding satellite faults to the south of the profile is a physical argument that justifies the electrical discontinuities between holes 1P1 and 2P1 and between holes 2P1 and 3P1. It is highly likely that because of the faulting in this corridor, the marl and limestone bedrock revealed by boreholes 1P1 and 2P1 may have risen. The rising bedrock prevented the basaltic flow from flowing southwards. Section GS1 has been correlated with data from borehole NIRE 254/30.

Section GS2 (Figure 7) groups the electrical soundings carried out in profile 3. It shows a gradual sinking of the marl and limestone bedrock towards the south, unlike the previous section, which generated a synclinal depression into which the basalts flowed with a thickness that increased from north to south. The existence of electrical discontinuities between boreholes 1P3 and 2P3 and between 2P3 and 3P3 corresponds to the continuity of NMAA satellite faults, leading to the uplift of the marl–limestone bedrock at the level of borehole 2P3, according to a horst structure, which prevented the flow of basaltic flows towards the south.

Section GS3 (Figure 8) at the level of profile 5, shows that the top of the marl–limestone bedrock forms a bowl structure where boreholes 4P5 and 5P5 show the lowest points. Towards the two north-western and south-eastern extremities, a rise in the roof is observed, which implies a decrease in the thickness of the overlying basaltic flows. A geophysical discontinuity was recorded between electrical boreholes 5P5 and 6P5, which may represent a fault or a simple flexure of the bedrock.

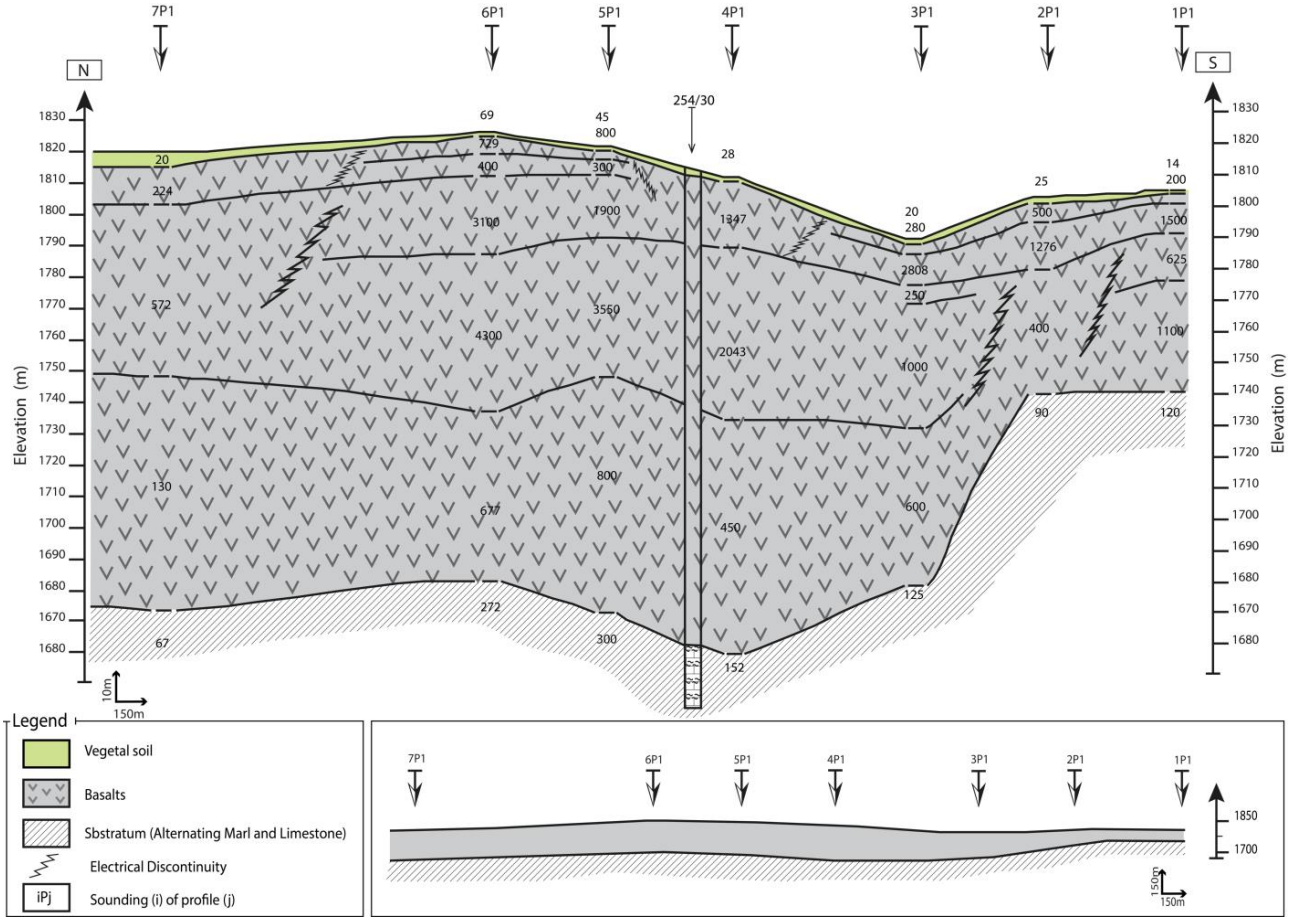

Figure 6. GS1 geoelectrical section of profile 1.

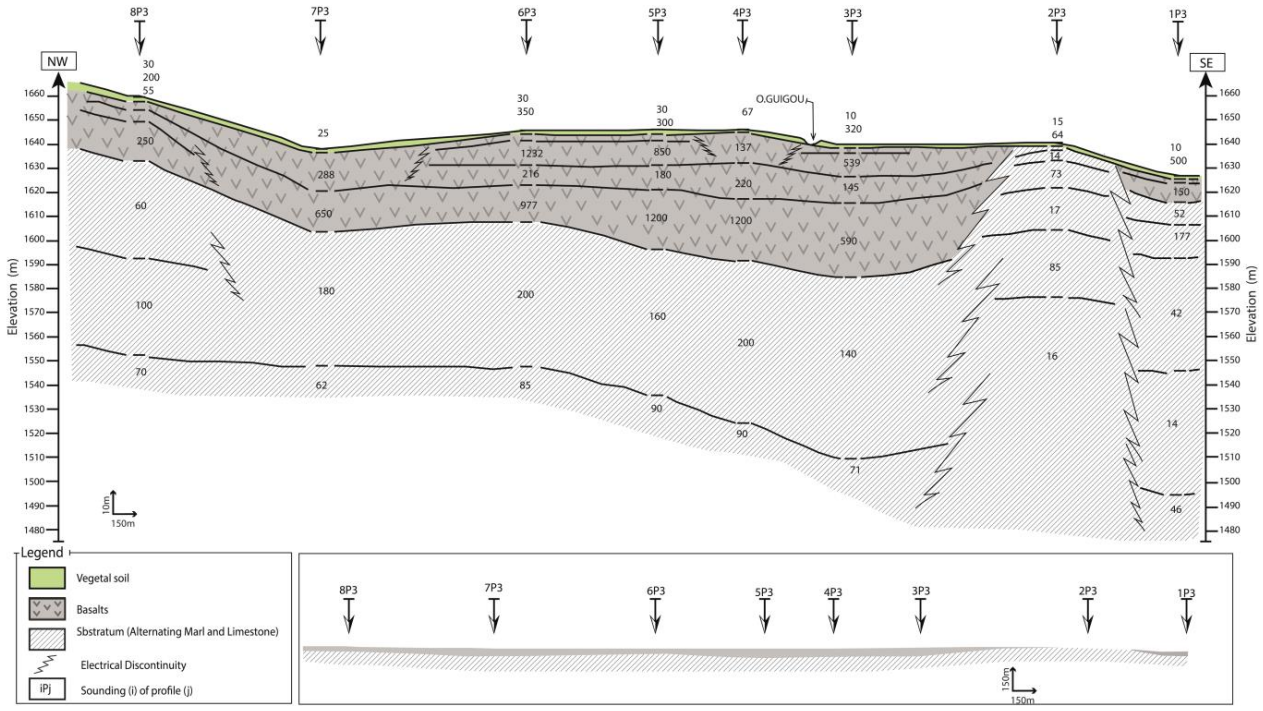

Figure 7. GS2 geoelectrical section of profile 3.

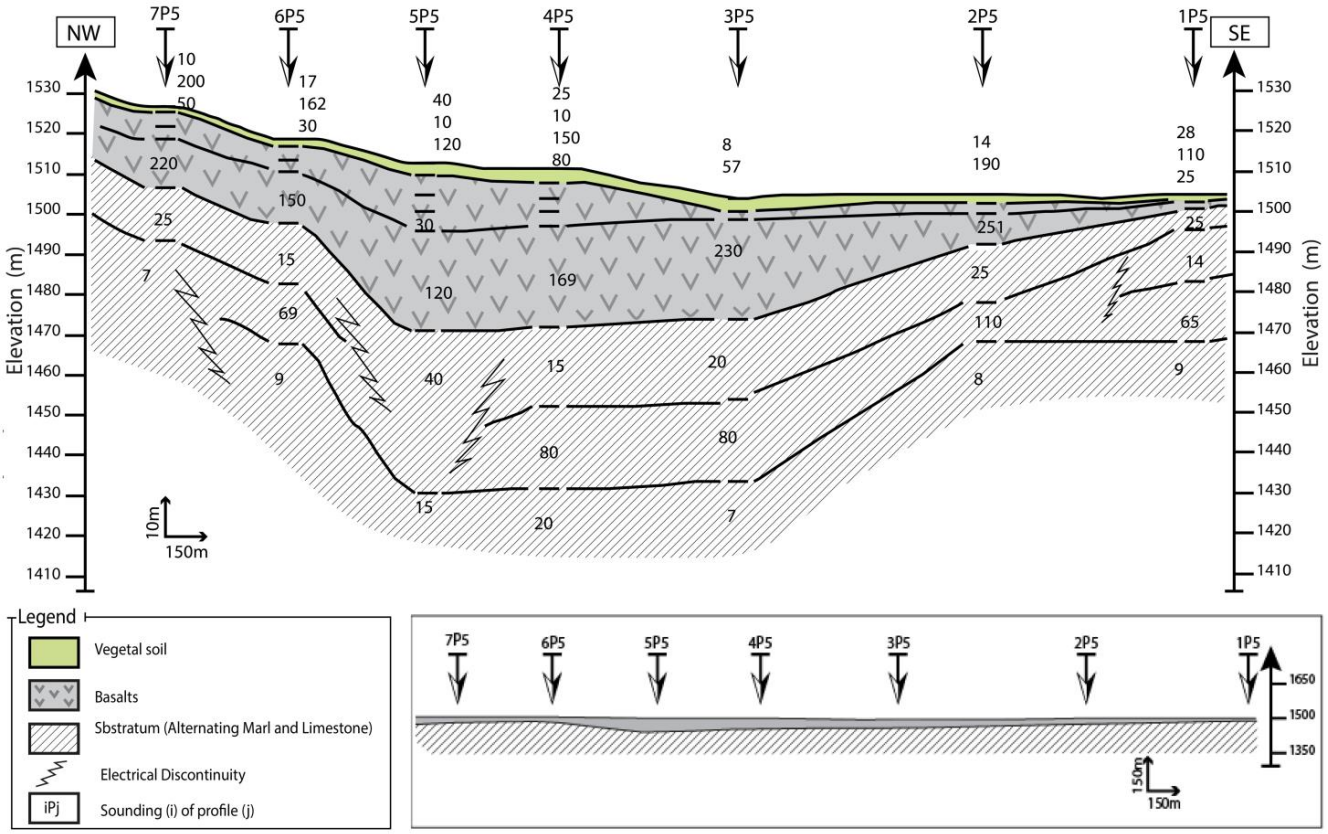

Figure 8. GS3 geoelectrical section of profile 5.

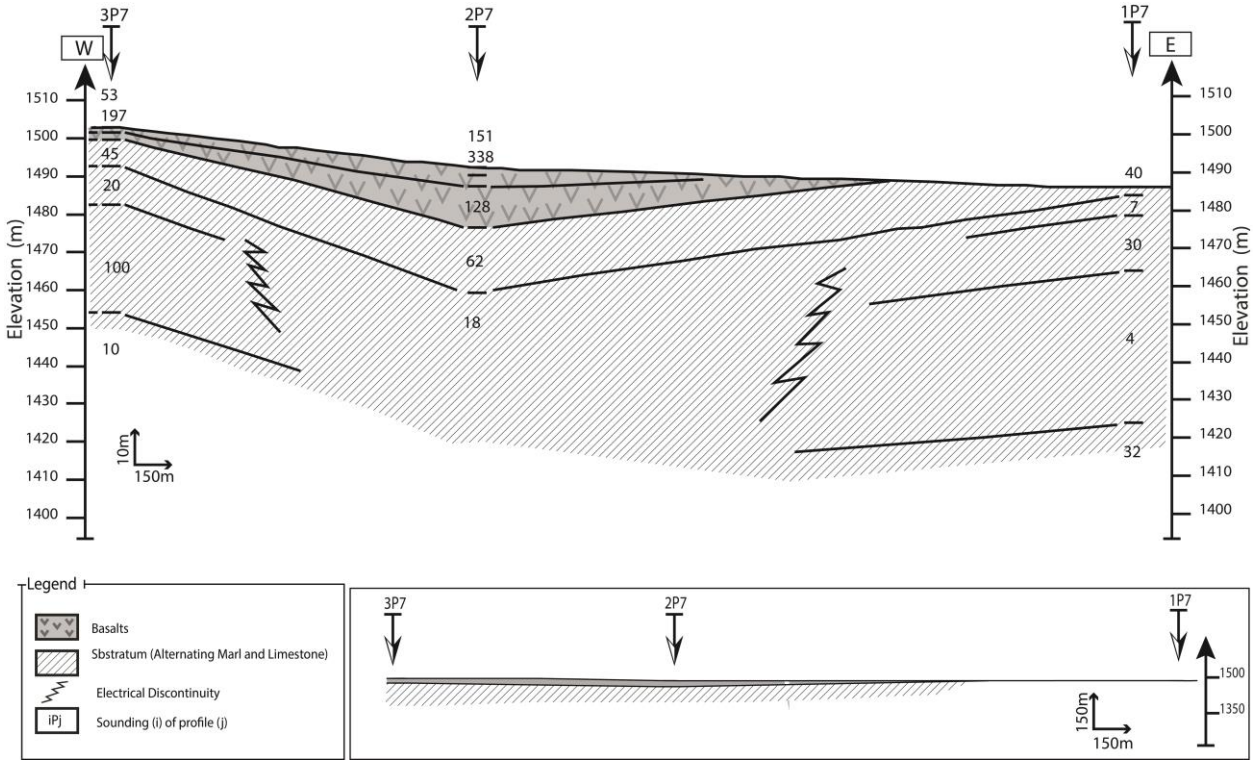

Figure 9. GS4 geoelectrical section of profile 7.

Section GS4 (Figure 9) is oriented E–W towards the north-eastern edge of the study area and follows profile 7. In this section, the thickness and extent of the basalts are clearly reduced. The maximum thickness reached by the basalts is 20 m, which was recorded in the middle of the section. Furthermore, a decrease in the thickness of these basalts is highlighted towards the west side where it reaches less than 5 m on the one hand. On the other hand, going towards the east end, this thickness progressively decreases until the bedrock outcrops.

4.3. Interpretative Map Analysis

The apparent iso-resistivity maps show the dispersion and lateral variation of the apparent resistivity (ρa) in the study area for different slices of the ground. Two iso-resistivity maps have been developed ($\rho a_{AB=80\,m}$ and $\rho a_{AB=200\,m}$). The analysis of the apparent resistivity map $\rho a_{AB=80\,m}$ presented in Figure 10a for a line length of AB = 80 m, corresponding to an investigation depth of about 15 m, allowed us to distinguish the following areas: (i) highly resistive areas (ρa >200 Ωm), corresponding to zones where the basalts are quite thick, notably in the SW of the study area; (ii) quite conductive areas ($\rho a \leq 100\ \Omega m$), located in the east and north-east of the study area. This decrease in apparent resistivity (ρa) is most probably linked to the absence of basalts on the surface; (iii) the rest of the map is occupied by intermediate resistivity ($100 \leq \rho a \leq 200\ \Omega m$), occupying large areas and corresponding to zones where basalts are present with small thicknesses, or they are more altered. For a deeper slice, the map $\rho a_{AB=200\,m}$ (Figure 10b) corresponds to a depth of investigation of about 30 m, and this map roughly follows the pattern of the previous map $\rho a_{AB=80\,m}$ and shows a very resistant zone ($\rho a \geq 500\ \Omega m$), located SE of the study area. This increase in ρa reflects the presence of very resistant terrain corresponding to basalts. A relatively conductive zone ($\rho a \leq 100\ \Omega m$) is located to the north-east of the surveyed area. This decrease in electrical resistivity is due to the presence of Pliocene marl and marl–limestone soils from the surface. The zones of intermediate resistivity ($100 \leq \rho a \leq 500\ \Omega m$) correspond to areas where the basalts are of low thickness above the Pliocene marl–limestone bedrock.

The isohypse map of the marl–limestone bedrock (Figure 10c) shows that the roof altitude varies between 1800 m, recorded at the upstream end of the plain, and 1460 m, the minimum value recorded downstream. It shows, in a general way, the behavior of the roof of the marly–limestone substratum, which gradually plunges from the south-west to the north-east in accordance with the flow of Oued Guigou and the water table. The isopach map represents the thickness distribution of the basaltic aquifer. The examination of this map (Figure 10d) shows that the maximum values are located to the south-west of the study area, mainly at the level of the electrical boreholes of profile 1 where the thickness values are close to 150 m. Overall, the thickness of the basaltic formations decreases progressively from the south-west to the north-east, with a slight increase in profiles 5 and 6.

4.4. Tectonic and Hydrogeological Implications

This work, based on geophysical reconnaissance by VES, shows the existence at depths of a more or less conductive level corresponding to calcareous marl alternations, surmounted by a very resistant level attributed to Quaternary basalts with a thickness that reaches at least 150 m in the south-western part of the study area. These thicknesses are consistent with those found by A. Bentayeb and C. Leclerc [38]. These basaltic formations have good hydrodynamic characteristics, which can yield significant flows depending on their degree of fracturing, and their rate of recharge [1].

The production of qualitative geoelectrical maps in terms of apparent resistivity made it possible to identify conductive areas and resistant areas that were interpreted differently according to the different lengths of the injection line. The conductive patches were attributed to the sub-cropping of the marl and limestone bedrock formations, while the resistant patches reflected the presence of fairly thick basalts. The quantitative isohypse map of the marl–limestone bedrock roof shows, as do the geoelectrical sections, that this

roof gradually dips from the south-west to the north-east. The maximum elevation of a roof at this level would be to the order of 1900 m towards the south-west of the surveyed area, and it records the coast of 1480 m towards the north-east with a difference in altitude of 420 m for a distance of 32,000 m and a gradient of 1.3%.

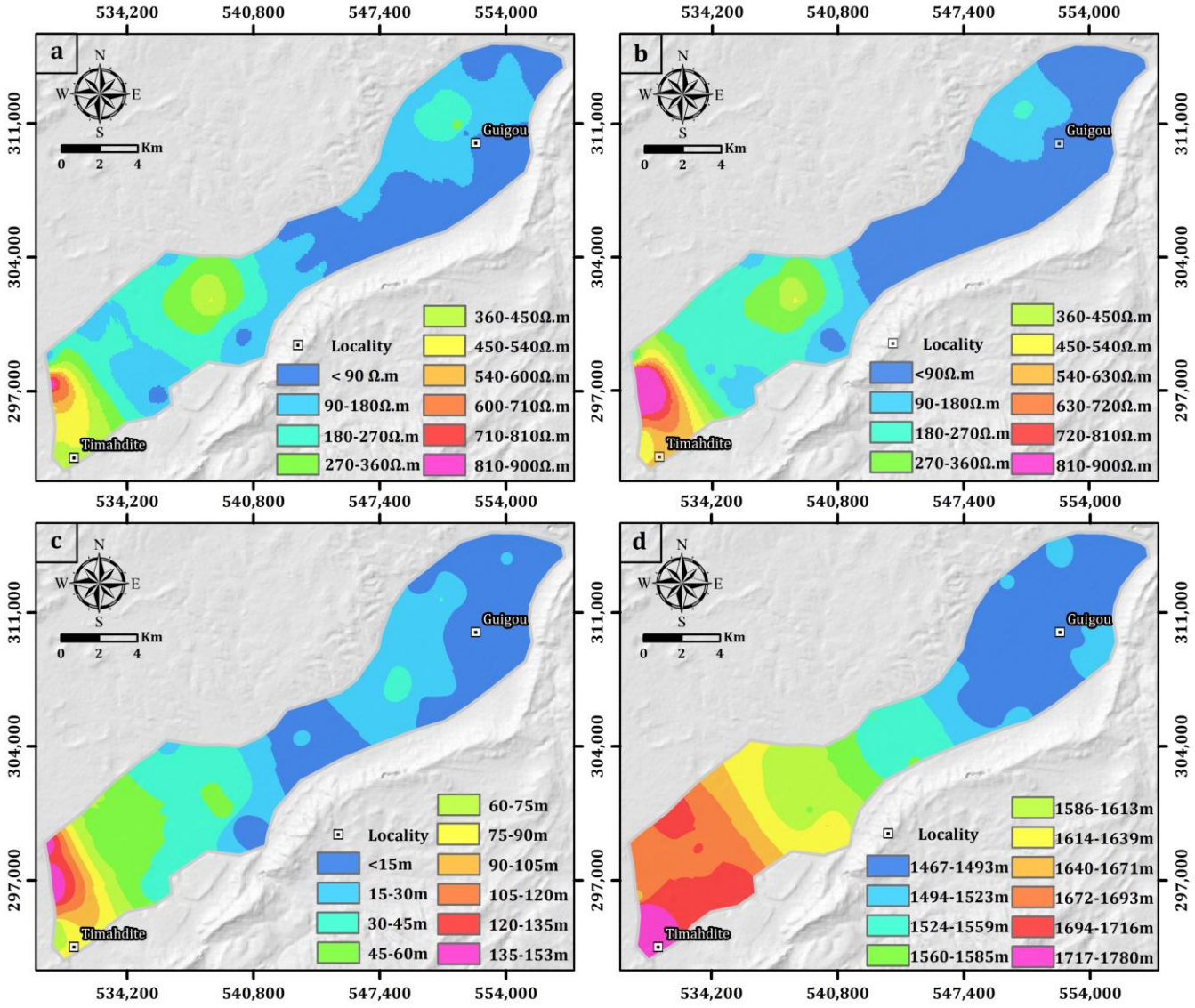

Figure 10. Thematic maps: (**a**): Apparent resistivity map for AB = 80 m (**b**): Apparent resistivity map for AB = 200 m (**c**): Isohypse map of the bedrock of marl and limestone (**d**): Map of Quaternary basalt isopach.

The main geoelectrical characteristics extracted from the geoelectrical sections and maps, coupled with the geological information available on this area, allowed us to elaborate on the aquifer prospectivity map presented in Figure 11. The alignment of electrical discontinuities allowed the continuity of lineaments between the geoelectrical sections to be estimated and the orientation and interpretation of these lineaments in terms of faults or fractures to be deduced. These fractures show a NE–SW direction sub-parallel to the major accidents of the Middle Atlas, highlighted by numerous old works [1,7]. The work of Amrani and Hinaj (2016) demonstrated that groundwater flows in the Plio-Quaternary aquifer system follow the NE–SW trend, with multi-gap faults affecting the collapsed zone of the Guigou Plain. In this sense, these physical discontinuities play a major hydrogeological role in the preferential circulation of groundwater. The local aquifer prospectivity map shown in Figure 11 outlines the potential alignment of regional faults deduced from the electrical

discontinuities (EDs). The zones of passage of these faults between the electrical sections are confirmed by the alignment of the boreholes with particularly good water flows.

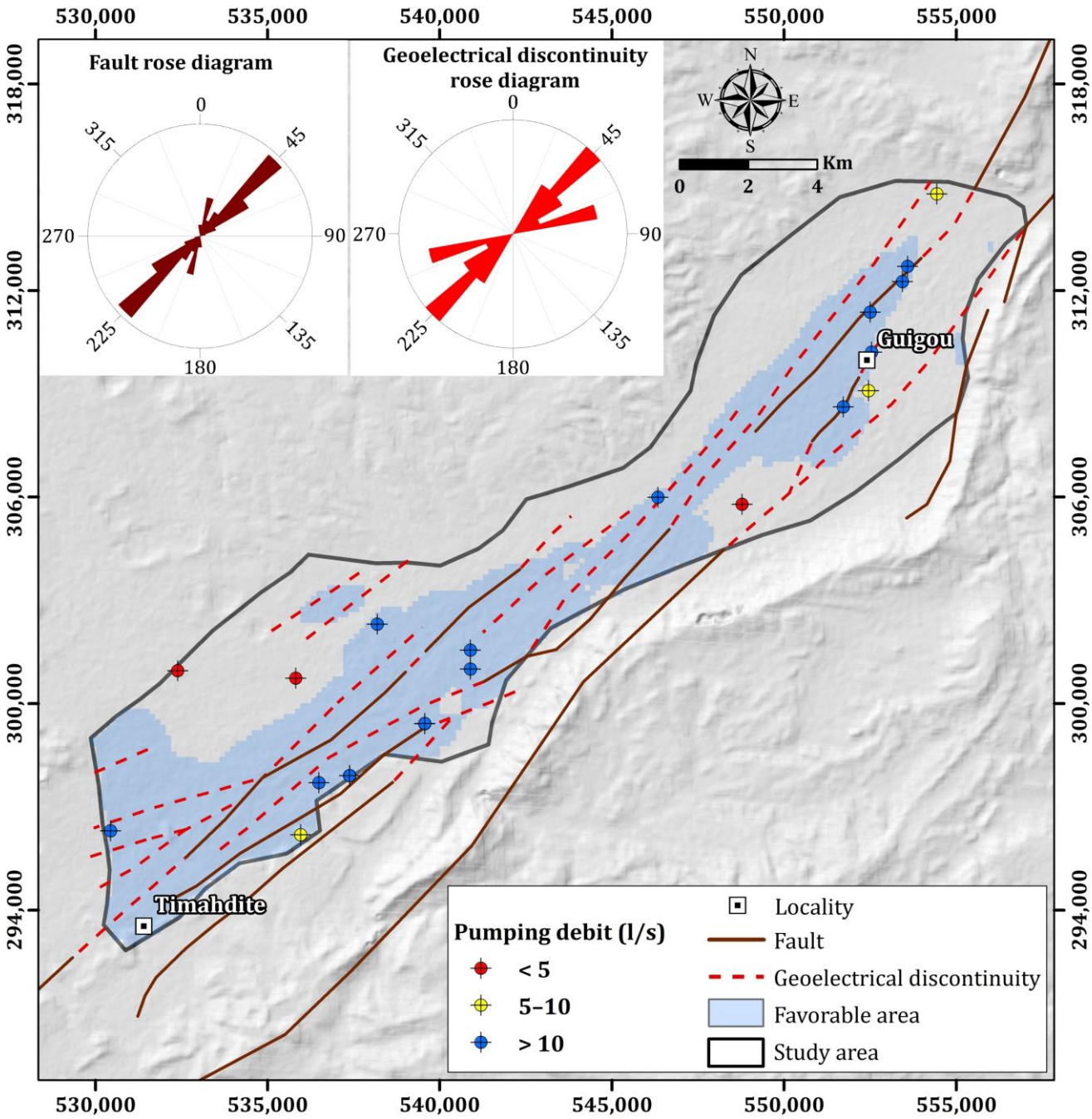

Figure 11. Aquifer prospectivity map showing the most favorable areas for drilling.

The lineaments in red correspond to the zones of passage of the electrical discontinuities. On the other hand, those in brown reflect the faulted structures as they are mapped on the ground from the structural and geological maps of the study area. Subsequently, the superposition of the results obtained allowed us to identify the most favorable areas for the installation of groundwater exploitation wells. To justify this choice, a hydrogeological survey was carried out, which showed that the position of the boreholes with a good flow rate ($Q > 10$ L/s) coincide with the favorable zones (see Figure 11). On the other hand, low-flow boreholes ($Q < 5$ L/s) are located far from favorable areas and medium-flow

boreholes (5 L/s < Q < 10 L/s) are located near favorable areas. The results of this study will serve as a guide to optimize the location of new wells and/or boreholes.

5. Conclusions

The present work demonstrates the importance of using VES geoelectrical data in the characterization of aquifers. This technique was applied to target areas of high groundwater-flow potential in the Guigou plain between the town of Timahdite and the village of Almis Guigou. The results obtained led to detailed map of the electrical discontinuities corresponding to fracture zones affecting the basalts forming the main aquifer. Iso-resistivity, the marl–limestone bedrock and basalt thickness maps were generated to characterize this aquifer.

The analysis and Interpretation of all the VES measurements show the presence of a very resistant upper level with a thickness varying between 0 and 150 m, attributed to the basaltic formations of the Quaternary age, followed by a moderately conductive horizon with a resistivity of about 90 Ωm. According to local geological data, this conductive level corresponds to Pliocene marl and limestone alternations. The correlation between the geophysical models obtained from the VES interpretations and their confrontation with local geological data and the lithological sections of the mechanical drillings made it possible to draw a certain number of geoelectrical sections, which reflect the evolution of the thickness and resistivity of the basalts above the marl–limestone bedrock. Indeed, the marl and limestone formations generally plunge from the south-west to the north-east with the presence of geophysical discontinuities, which locally interrupt this plunge. These detected electrical discontinuities could be interpreted in terms of a manifestation of the scarping of the satellite faults of the North Middle Atlas accident, which blocked the flow of basalts southwards and formed this basaltic aquifer, preventing the flow of basalts.

The integration of geophysical and geological field knowledge has led to a more informed regional tectonic interpretation and assessment of the hydrogeological prospects of the region. To this end, the results of this geophysical survey have made it possible to better characterize the geometry of the Quaternary basaltic aquifer and the electrical discontinuities and its Pliocene calcareous marl substratum. Thus, this study constitutes a basic document to help decision makers better manage the siting of water boreholes in order to ensure the good integrated management of the region's groundwater resources.

Author Contributions: Conceptualization, S.E.M., A.R., A.M. and M.B.; Methodology, S.E.M., Y.M., A.M. and A.R.; Software, S.E.M., Y.M., A.R. and A.M.; Validation, S.E.M., Y.M., G.R., M.B. and A.M.; Formal analysis, S.E.M., Y.M., H.E.M., A.A., A.M. and A.R.; Investigation, S.E.M., M.E.H., S.L. and A.M.; Resources, A.M.; Data curation, S.E.M., Y.M., H.E.M., A.A. and A.M.; Writing—original draft, S.E.M., Y.M., A.M. and H.E.M.; Writing—review & editing, S.E.M. and A.M.; Visualization, S.E.M., G.R., M.E.H., A.M. and M.B.; Supervision, M.B.; Project administration, M.B.; Funding acquisition, A.M. All authors have read and agreed to the published version of the manuscript.

Funding: This research received no external funding.

Institutional Review Board Statement: Not applicable.

Informed Consent Statement: Not applicable.

Data Availability Statement: Not applicable.

Acknowledgments: The authors would like to thank the Editors of the Special Issue as well as the anonymous reviewers for their valuable comments on this article, which allowed us to improve the scientific quality of this research.

Conflicts of Interest: The authors declare no conflict of interest.

References

1. Amrani Hydrodynamisme. Hydrogéochimie et Vulnérabilité de La Nappe d'Eau Superficielle et Leur Relation Avec La Tectonique Cassante Dans La Zone Effondrée Timahdite—Almis Guigou (Moyen Atlas, Maroc). Available online: http://www.secheresse.info/spip.php?article845642016 (accessed on 1 December 2022).
2. Todd, D.K.; Mays, L.W. *Groundwater Hydrology*; John Wiley & Sons: Hoboken, NJ, USA, 2004; ISBN 0471059374.
3. Fetter, C.W. *Applied Hydrogeology*; Waveland Press: Long Grove, IL, USA, 2018; ISBN 1478637447.
4. Jha, M.K.; Kumar, S.; Chowdhury, A. Vertical Electrical Sounding Survey and Resistivity Inversion Using Genetic Algorithm Optimization Technique. *J. Hydrol.* **2008**, *359*, 71–87. [CrossRef]
5. Raju, N.J.; Reddy, T.V.K. Fracture Pattern and Electrical Resistivity Studies for Groundwater Exploration. *Environ. Geol.* **1998**, *34*, 175–182. [CrossRef]
6. Mohamed, A.; Al Deep, M.; Othman, A.; Taha Al Alshehri, F.; Abdelrady, A. Integrated Geophysical Assessment of Groundwater Potential in Southwestern Saudi Arabia. *Front. Earth Sci* **2022**, *10*, 937402. [CrossRef]
7. Hinaje, S. Tectonique Cassante et Paléochamps de Contraintes Dans Le Moyen Atlas et le Haut Atlas Central (Midelt-Errachidia) Depuis Le Trias Jusqu'à l'actuel. Unpublished Thesis, Mohamed V University, Rabat, Morocco, 2004.
8. Christensen, N.B.; Christiansen, A. V Using Geophysical Survey Results in the Inference of Aquifer Vulnerability Measures. *Near Surf. Geophys.* **2021**, *19*, 505–521. [CrossRef]
9. Bangalore Nagaraj, P.; Mandalagiri Subbarayappa, M.K.; Jean-Michel, V.; Hoareau, J. Estimation of Anisotropic Hydraulic Conductivity Using Geophysical Data in a Coastal Aquifer of Karnataka, India. *Hydrol. Process.* **2021**, *35*, e14395. [CrossRef]
10. Nugraha, G.U.; Nur, A.A.; Pranantya, P.A.; Lubis, R.F.; Bakti, H. Analysis of Groundwater Potential Zones Using Dar-Zarrouk Parameters in Pangkalpinang City, Indonesia. *Environ. Dev. Sustain.* **2022**, 1–23. [CrossRef]
11. Puttiwongrak, A.; Men, R.; Vann, S.; Hashimoto, K.; Suteerasak, T. Application of Geoelectrical Survey and Time-Lapse Resistivity with Groundwater Data in Delineating a Groundwater Potential Map: A Case Study from Phuket Island, Thailand. *Sustainability* **2022**, *14*, 397. [CrossRef]
12. Rhubango, H.-A.; Mwangaza, N. Geo-Electrical Investigation for Groundwater Resources in a Part of Butembo Area (North Kivu Province; Democratic Republic of Congo). *Am. Acad. Sci. Res. J. Eng. Technol. Sci.* **2022**, *85*, 157–169.
13. Essahlaoui, A.; Sahbi, H.; El Yamine, N. Application de La Géophysique (Méthode Géoélectrique) à La Reconnaissance Du Plateau de Meknès (Bassin de Saïss), Maroc. *Geol. Belg.* **2000**. [CrossRef]
14. Tijani, M.N.; Obini, N.; Inim, I.J. Estimation of Aquifer Hydraulic Parameters and Protective Capacity in Basement Aquifer of South-Western Nigeria Using Geophysical Techniques. *Environ. Earth Sci.* **2021**, *80*, 466. [CrossRef]
15. Ben Fraj, A.; Gabtni, H. Quaternary Alluvial Aquifer Study Using Integrated Geophysical Approach in Zaghouan Plain (North-eastern Tunisia). *Nat. Resour. Res.* **2021**, *30*, 307–319. [CrossRef]
16. Mohamed, A.; Gonçalvès, J. Hydro-Geophysical Monitoring of the North Western Sahara Aquifer System's Groundwater Resources Using Gravity Data. *J. Afr. Earth Sci.* **2021**, *178*, 104188. [CrossRef]
17. Obiora, D.N.; Ibuot, J.C. Geophysical Assessment of Aquifer Vulnerability and Management: A Case Study of University of Nigeria, Nsukka, Enugu State. *Appl. Water Sci.* **2020**, *10*, 29. [CrossRef]
18. Doetsch, J.; Linde, N.; Coscia, I.; Greenhalgh, S.A.; Green, A.G. Zonation for 3D Aquifer Characterization Based on Joint Inversions of Multimethod Crosshole Geophysical Data. *Geophysics* **2010**, *75*, G53–G64. [CrossRef]
19. Bayowa, O.G.; Afolabi, O.A.; Akinluyi, F.O.; Oshonaiye, A.O.; Adelere, I.O.; Mudashir, A.W. Integrated Geoelectrics and Hydrogeochemistry Investigation for Potential Groundwater Contamination around a Reclaimed Dumpsite in Taraa, Ogbomoso, Southwestern Nigeria. *Int. J. Energy Water Resour.* **2022**, 1–22. [CrossRef]
20. Azffri, S.L.; Azaman, A.; Sukri, R.S.; Jaafar, S.M.; Ibrahim, M.F.; Schirmer, M.; Gödeke, S.H. Soil and Groundwater Investigation for Sustainable Agricultural Development: A Case Study from Brunei Darussalam. *Sustainability* **2022**, *14*, 1388. [CrossRef]
21. Ebraheem, A.A.; Sherif, M.; Mulla, M.A.; Alghafli, K.; Sefelnasr, A. Assessment of Groundwater Resources in Water Spring Areas Using Geophysical Methods, Northern UAE. In *Wadi Flash Floods*; Springer: Singapore, 2022; pp. 493–508.
22. Shishaye, H.A.; Tait, D.R.; Befus, K.M.; Maher, D.T. An Integrated Approach for Aquifer Characterization and Groundwater Productivity Evaluation in the Lake Haramaya Watershed, Ethiopia. *Hydrogeol. J.* **2019**, *27*, 2121–2136. [CrossRef]
23. Hamzah, U.; Samsudin, A.R.; Malim, E.P. Groundwater Investigation in Kuala Selangor Using Vertical Electrical Sounding (VES) Surveys. *Environ. Geol.* **2007**, *51*, 1349–1359. [CrossRef]
24. Troisi, S.; Fallico, C.; Straface, S.; Migliari, E. Application of Kriging with External Drift to Estimate Hydraulic Conductivity from Electrical-Resistivity Data in Unconsolidated Deposits near Montalto Uffugo, Italy. *Hydrogeol. J.* **2000**, *8*, 356–367. [CrossRef]
25. Mamouch, Y.; Attou, A.; Miftah, A.; Ouchchen, M.; Dadi, B.; Achkouch, L.; Et-tayea, Y.; Allaoui, A.; Boualoul, M.; Randazzo, G.; et al. Mapping of Hydrothermal Alteration Zones in the Kelâat M'Gouna Region Using Airborne Gamma-Ray Spectrometry and Remote Sensing Data: Mining Implications (Eastern Anti-Atlas, Morocco). *Appl. Sci.* **2022**, *12*, 957. [CrossRef]
26. Bernini, M.; Boccaletti, M.; Gelati, R.; Moratti, G.; Papani, G.; Mokhtari, J. El Tectonics and Sedimentation in the Taza-Guercif Basin, Northern Morocco: Implications for the Neogene Evolution of the Rif-Middle Atlas Orogenic System. *J. Pet. Geol.* **1999**, *22*, 115–128. [CrossRef]
27. Termier, H. Etudes Géologiques Sur Le Maroc Central et Le Moyen-Atlas Septentrional. 1936. Available online: https://www.persee.fr/doc/rga_0035-1121_1937_num_25_3_3982_t1_0525_0000_1 (accessed on 1 December 2022).

28. Colo, G. Contribution a L'étude Du Jurassique Du Moyen Atlas Septentrional: Atlas de Planches Hors Texte; Éd. de la Division de la géologie, Direction, Ministère, Royaume du Maroc. 1961. Available online: https://bibliotheques.mnhn.fr/medias/detailstatic.aspx?INSTANCE=exploitation&RSC_BASE=HORIZON&RSC_DOCID=379840 (accessed on 1 December 2022).
29. Gentil, L. Notice Sur Les Titres et Travaux Scientifiques, E. Larose. 1918. Available online: https://gallica.bnf.fr/ark:/12148/bpt6k90008k.texteImage (accessed on 1 December 2022).
30. Martin, J. Le Moyen Atlas Central, Étude Géomorphologique. 1981. Available online: http://pascal-francis.inist.fr/vibad/index.php?action=getRecordDetail&idt=PASCALGEODEBRGM8220223851 (accessed on 1 December 2022).
31. Dresnay, R. du Recent Data on the Geology of the Middle-Atlas (Morocco). In *The Atlas System of Morocco*; Springer: Berlin/Heidelberg, Germany, 1988; pp. 293–320.
32. Sachse, V.F.; Leythaeuser, D.; Grobe, A.; Rachidi, M.; Littke, R. Organic Geochemistry and Petrology of a Lower Jurassic (Pliensbachian) Petroleum Source Rock from Aït Moussa, Middle Atlas, Morocco. *J. Pet. Geol.* **2012**, *35*, 5–23. [CrossRef]
33. Termier, H.; Dubar, G. *Carte Géologique Provisoire Du Moyen-Atlas Septentrional Au 1/200.000 e: Notice Explicative*; Imprimerie Officielle: Radès, Tunisia, 1940.
34. Charroud, M. Evolution Géodynamique de La Partie Sud-Ouest Du Moyen Atlas Durant Le Passage Jurassique-Crétacé, Le Crétacé et Le Paléogène: Un Exemple d'évolution Intraplaque. These 3eme Cycle. Université Mohammed V, Rabat, Morocco, 1990.
35. Ouarhache, D.; Charriere, A.; Chalot-Prat, F.; Wartiti, M.E.L. Triassic to Early Liassic Continental Rifting Chronology and Process at the Southwest Margin of the Alpine Tethys (Middle Atlas and High Moulouya, Morocco); Correlations with the Atlantic Rifting, Synchronous and Diachronous. *Bull. Société Géologique Fr.* **2012**, *183*, 233–249. [CrossRef]
36. Hamidi, E.M.; Boulangé, B.; Colin, F. Altération d'un Basalte Triasique de La Région d'Elhajeb, Moyen Atlas, Maroc. *J. Afr. Earth Sci.* **1997**, *24*, 141–151. [CrossRef]
37. Muzirafuti, A.; Boualoul, M.; Barreca, G.; Allaoui, A.; Bouikbane, H.; Lanza, S.; Crupi, A.; Randazzo, G. Fusion of Remote Sensing and Applied Geophysics for Sinkholes Identification in Tabular Middle Atlas of Morocco (the Causse of El Hajeb): Impact on the Protection of Water Resource. *Resources* **2020**, *9*, 51. [CrossRef]
38. Bentayeb, A.; Leclerc, C. Le Causse Moyen Atlasique. In *Ressources en Eaux du Maroc, Tome3, Domaines Atlasiques Sud-Atlasiques*; 1977; pp. 37–66. Available online: https://www.scribd.com/document/494028246/Ressources-en-Eau-Du-MAROC-Tome-III (accessed on 1 December 2022).
39. Ellouz, N.; Patriat, M.; Gaulier, J.-M.; Bouatmani, R.; Sabounji, S. From Rifting to Alpine Inversion: Mesozoic and Cenozoic Subsidence History of Some Moroccan Basins. *Sediment. Geol.* **2003**, *156*, 185–212. [CrossRef]
40. Arboleya, M.L.; Teixell, A.; Charroud, M.; Julivert, M. A Structural Transect through the High and Middle Atlas of Morocco. *J. Afr. Earth Sci.* **2004**, *39*, 319–327. [CrossRef]
41. Gomez, F.; Barazangi, M.; Bensaid, M. Active Tectonism in the Intracontinental Middle Atlas Mountains of Morocco: Synchronous Crustal Shortening and Extension. *J. Geol. Soc. Lond.* **1996**, *153*, 389–402. [CrossRef]